2015

Improvements in the dispersion of nanosilver in a MgB2 matrix through a graphene oxide net

Mislav Mustapic
University of Wollongong, mislav@uow.edu.au

Kaludewa S. B. De Silva
University of Wollongong, kaludewa@uow.edu.au

Seyed H. Aboutalebi
University of Wollongong, sha942@uowmail.edu.au

Shaon Barua
University of Wollongong, sb201@uowmail.edu.au

Xun Xu
University of Wollongong, xun@uow.edu.au

See next page for additional authors

Improvements in the dispersion of nanosilver in a MgB2 matrix through a graphene oxide net

Abstract

The effects of graphene oxide (GO) addition on the dispersion of nanosilver (Ag) in an MgB2 matrix were studied using bulk samples prepared through a diffusion process. The influence of the dispersion of Ag and Ag/GO particles on the critical current density (Jc) of MgB2 was also investigated. GO has emerged as an excellent dopant which can significantly improve both the low- and high-field performance of MgB2 due to its capability to improve intergrain connectivity (GO) and inter- and intragrain pinning (GO and AgMg). The addition of nanosize Ag particles also results in an improvement of vortex pinning, and at the same time, it offers the advantage of preventing the loss of Mg during the sintering process. It is found that the dispersion of nanosilver in the presence of GO results in significant improvements in the critical current density in MgB2, particularly at high magnetic fields, due to improved intergrain connectivity and flux pinning. The use of the GO net as a platform for doping MgB2 in our case with Ag yielded a 10-fold-better critical current density (Jc) than standard Ag doping at 9 T and 5 K. Even without sophisticated processes, we obtained a Jc result of 10^4 A/cm^2 at 9 T and 5 K, which is one of the best ever achieved.

Disciplines

Engineering | Science and Technology Studies

Authors

Mislav Mustapic, Kaludewa S. B. De Silva, Seyed H. Aboutalebi, Shaon Barua, Xun Xu, Jianli Wang, Md Shariar Hossain, Josip Horvat, and Shi Xue Dou

Improvements in Dispersion of Nano-Silver in MgB$_2$ Matrix through Graphene Oxide Net

Mislav Mustapić[a*], Kaludewa S. B. De Silva[a,b], Seyed H. Aboutalebi[a], Shaon Barua[a], Xun Xu[a], X. L. Wang, Md Shariar Hossain[a], Josip Horvat[a], Shi Xue Dou[a]

[a] **Institute for Superconducting and Electronic Materials, AIIM, University of Wollongong, Squires Way, North Wollongong, NSW 2500, Australia**
[b] **Institute for Nanoscale Technology, Faculty of Science, University of Technology Sydney, City Campus, PO Box 123, Broadway, NSW 2007, Australia**

Corresponding author: mislav@uow.edu.au

ABSTRACT:

The effects of graphene oxide (GO) addition on the dispersion of nano-silver (Ag) in an MgB$_2$ matrix were studied using bulk samples prepared through a diffusion process. The influence of the dispersion of Ag and Ag/GO particles on the critical current density (J$_C$) of MgB$_2$ was also investigated. GO has emerged as an excellent dopant which can significantly improve both low- and high- field performance of MgB$_2$ due to its capability to improve inter-grain connectivity (GO), and inter- and intra-grain pinning (GO and AgMg). The addition of nano-size Ag particles also results in improvement of vortex pinning, and at the same time, it offers the advantage of preventing the loss of Mg during the sintering process. It is found that dispersion of nano-silver in the presence of GO results in significant improvements to the critical current density in MgB$_2$, particularly at high magnetic fields, due to improved inter-grain connectivity and flux pinning. The use of the GO net as a platform for doping MgB$_2$ in our case with Ag, yielded a 10 times better critical current density (J$_C$) than standard Ag doping at 9 T and 5 K. Even without sophisticated processes, we obtained J$_C$ result of 10^4 A/cm^2 at 9 T and 5 K, which is one of the best ever achieved.

1. Introduction:

Since the discovery of superconductivity in MgB_2[1], extensive research has been undertaken to enhance its superconducting properties, such as its critical current density (J_C), upper critical field (H_{c2}), and irreversibility field (H_{irr}). The incorporation of nano size carbon containing dopants such as SiC, carbon nanotubes (CNT), malic acid, graphene, and graphene oxide into this superconductor has been reported widely as being an effective means of improving the superconducting properties[2-6]. Most carbon dopants, however, have adverse effects on the critical temperature (T_c) and the low field J_C performance. Among these, graphene oxide (GO) has been recognized as an outstanding dopant for MgB_2 due to its capability to improve both low and high field performance, at very low doping levels[7].

The optimization of the stoichiometry of Mg and B has played a vital role in the fabrication of this superconductor, as its microstructure and superconducting properties are greatly affected by the Mg/B ratio[8]. Controlling the Mg/B ratio during sintering is difficult due to the inevitable vaporization of Mg during the sintering process. Usually 20% excess Mg is added to compensate the Mg loss during the diffusion sintering process. Nano-silver addition has been reported as an effective sintering aid to facilitate good control during the sintering process. Furthermore, it has been reported that the resultant nano scale Ag-Mg impurity phases encourage flux pinning resulting in improved superconducting performance at high field[9,10]. The use of nano-silver prepared in-house through chemical synthesis allowed us to incorporate optimized nano-Ag particles into the MgB_2 matrix. In this work, we report a significant improvement of J_C in MgB_2, with co-doping by graphene oxide and nano-Ag.

Previous studies have indicated that GO doped to MgB_2 did not show any negative impact on the connectivity of MgB_2 grains. Furthermore, recent researches present that GO doping even stimulate the growth of MgB_2 grains along preferred crystalline orientations[6,7] and improves the grain connectivity. It was also noticed that layered nano-sheets of GO are uniformly

spread within and among the MgB_2 crystals[6]. This behaviour of GO in the MgB_2 matrix makes it suitable as a platform for more effective doping of MgB_2 by other (previously used) elements and compounds. This produces a synergetic effect of localized atomic (carbon and oxygen) doping and texturing of the crystals (by GO) that significantly enhances both low and high field J_C. A considerable difference is noticeable between GO doping and doping with other carbon sources, such as graphene or CNT. Doping with graphene and CNT has negative effects on J_C in low magnetic fields due to an increase in disorder in the texturing of MgB_2, reducing conductivity between MgB_2 grains[11]. Even a small amount of carbon doping (1 wt%) has negative effects on J_C in low applied magnetic field due to quick reaction between carbon and boron.

The procedure for nano-Ag and GO co-doping of MgB_2 has been developed in this paper. The influence of nano-Ag doping in the presence of GO on the critical temperature, resistivity, grain to-grain connectivity, lattice disorder, and critical fields has also been investigated. The results are compared with those on non-doped samples and the origin of the difference in the critical current density is discussed. Finally, the effect of the silver nanoparticle dispersion in MgB_2 and the following enhancement of J_C is compared with previous research by other groups.

1.1. Ag doping by other research groups

Over the last decade and more, several groups have investigated the influence of Ag doping on MgB_2 electromagnetic performance. According to the earliest research, silver doping presents only a small impact on the resistivity characteristic of MgB_2. At the same time, many groups have focused on phase formation and the chemistry between elements. The microstructure approach provides vital information about the formation of new phases, temperature dependence, and the special distribution of phases during processing. Because it was a promising candidate, some researchers prepared thin films and polycrystals of MgB_2,

and used different techniques for the preparation of samples, such as the high pressure and diffusion methods.

Firstly Sun et al.[12] in 2002 reported the formation of the binary compound $Mg_{0.5}Ag_{0.5}$. Resistivity measurement showed the surprising result that T_c remained close to 39K even with increased doping by Ag. The J_C results did not show any significant improvement.

In the same year, Zouaoui et al.[13] prepared polycrystalline MgB_2 doped with various amounts of Ag. In summary, they demonstrated that MgB_2 with silver admixture shows relatively improved superconducting performance characterized by (a) slightly higher transition temperature, (b) lower absolute resistivity in the normal state with a linear T_C dependence, and (c) higher RRR. Also, they concluded that Ag reacts with excess magnesium and forms intermetallic layers of AgMg that cluster at crystallite boundaries, preventing the formation of MgB_2 and inducing disorder in the crystal structure.

Toulemonde et al.[14] investigated the superconducting properties of bulk samples prepared at high applied pressure for several dopant elements (Na, Ca, Cu, Ag, Zn, and Al). Among the above-mentioned dopant elements, Ag doping did not present results worthy of further investigation.

Kumar et al.[15] synthesised silver doped MgB_2 bulk samples. Their report mentions prevention of Mg loss at higher sintering temperature as well as the formation of pinning centres. Nevertheless, the results of critical current density obtained in their work showed lower values than the highest reported in the literature.

Song and co-workers[16] doped MgB_2 with Ag nanoparticles 30 nm in size and sintered it at the relatively high temperature of 900°C for 2 h. The XRD results were in agreement with most of those from previous research groups, with the formation of various impurity phases, such as the binary compounds MgAg, MgB_4, MgB_6, and MgO. They reported an enhancement of J_C with the Ag doping, and the optimal flux-pinning effect was obtained for 8 wt% Ag. Later,

a systematic investigation was carried out by Shekar et al.[9] on the effect of Ag doping on MgB$_2$. By using the same sintering conditions for all doping levels, an optimum J$_C$ was obtained for 10 at.%, which is in good agreement with Song et al.. The high value of J$_C$ for Ag-added MgB$_2$ superconductor was attributed to the inclusion of MgAg nanoparticles (5–20 nm) in the crystal matrix of MgB$_2$.

Kumakura and co-workers[17] were focused on the mechanism of reaction and phase formation related to Ag doping. They reported that the optimal silver addition level for high critical current properties is 2–5% against magnesium, which are much lower levels compared to the eutectic composition of the Mg–Ag system. Their research revealed that the synthesis temperature could be lowered down to 450°C by ~2% silver addition to magnesium, forming a eutectic system. Finally, they concluded that among many candidates for dopants, silver can improve the reactivity of magnesium through decreasing its melting point.

Kimishima et al.[18] mostly investigated J$_C$ of doped MgB$_2$ prepared from a sintered mixture of Mg, B, and Ag$_2$O in H$_2$ 10%/Ar atmosphere. They reported Ag–Mg nanoparticles with diameters of 10–15 nm that acted as pinning centres for magnetic flux penetrating into MgB$_2$. Their obtained J$_C$ values at 20 K and 1 T were estimated as 3.2×10^4, 4.2×10^4, and 3.6×10^4 A/cm^2 for the x = 0.01 and 0.02 samples, respectively.

Finally, Ranot et al.[19] prepared thin films of MgB$_2$ doped separately with Ag and Cu. They reported a significant enhancement of J$_C$ without suppression of T$_C$. The increase in J$_C$ resulted from improved grain connectivity and strong flux pinning by the high density of grain boundaries. The Ag doping was more effective than the Cu doping for J$_C$ enhancement in MgB$_2$ films.

All this work indicates on suitability of Ag for improvement of superconducting properties of MgB$_2$. The use of GO as a means of their dispersion and a potential source of additional carbon doping is investigated in this report.

2. Experimental procedures:

2.1. Sample preparation

The sample preparation steps are presented in Fig. 1, which are divided into three parts: synthesis of Ag nanoparticles, their attachment to GO sheets and preparation of MgB_2 by the diffusion method. Silver nanoparticles were synthesised by a wet technique with chemical reduction of silver salts. Approximately 3.5 mmol $Ag(NO_3)$ salt was dissolved in 30 ml deionised (DI) water (Fig. 1). In a separate three-necked beaker, 1 ml (31 mmol) of hydrazine was dissolved in 30 ml DI water, with a few droplets of ethylenediamine to provide an alkaline environment (pH $\approx$ 10). In this synthesis, no surfactant was used to prevent repulsion between Ag nanoparticles and GO sheets. Excess reducing agent (10 times greater concentration than silver salt) and an alkaline environment provide the best conditions for rapid and strong reduction of silver salts.

GO nano-sheets were mixed with freshly prepared Ag nanoparticles. The preparation procedure for GO in tetrahydrofuran (THF) solution was reported earlier[7]. This mixture was vigorously stirred for 2 hours. Finally, Ag/GO nanoparticles were centrifuged and dried in oven overnight at 75°C in low oxygen atmosphere.

Non-doped and doped bulk MgB_2 samples were prepared via the diffusion method. After a systematic study of Ag doping into MgB_2, [9,10] 5 wt. % nano-Ag was selected as the optimum Ag addition to the MgB_2 matrix. The 1 wt% GO doping level was selected as the optimum level for GO doping, based on our previous studies[7]. The co-doped sample was prepared through adding these two optimum quantities of Ag and GO, together with the B powder (99.999%, 0.2 to 2.4 μm in size). Powders were mixed thoroughly using a mortar and pestle, and were pressed into pellets 13 mm in diameter. The pellets were inserted into a soft iron tube with Mg powder (99%, 352 mesh) separated from the pellets and in quantity exceeding (+20%) the stoichiometric ratio of MgB_2 to account for its loss during heat treatment. The

samples were heat treated at 800°C for 10 hours in a quartz tube at a heating rate of 5°C min^{-1} under 99.9% pure flowing argon gas.
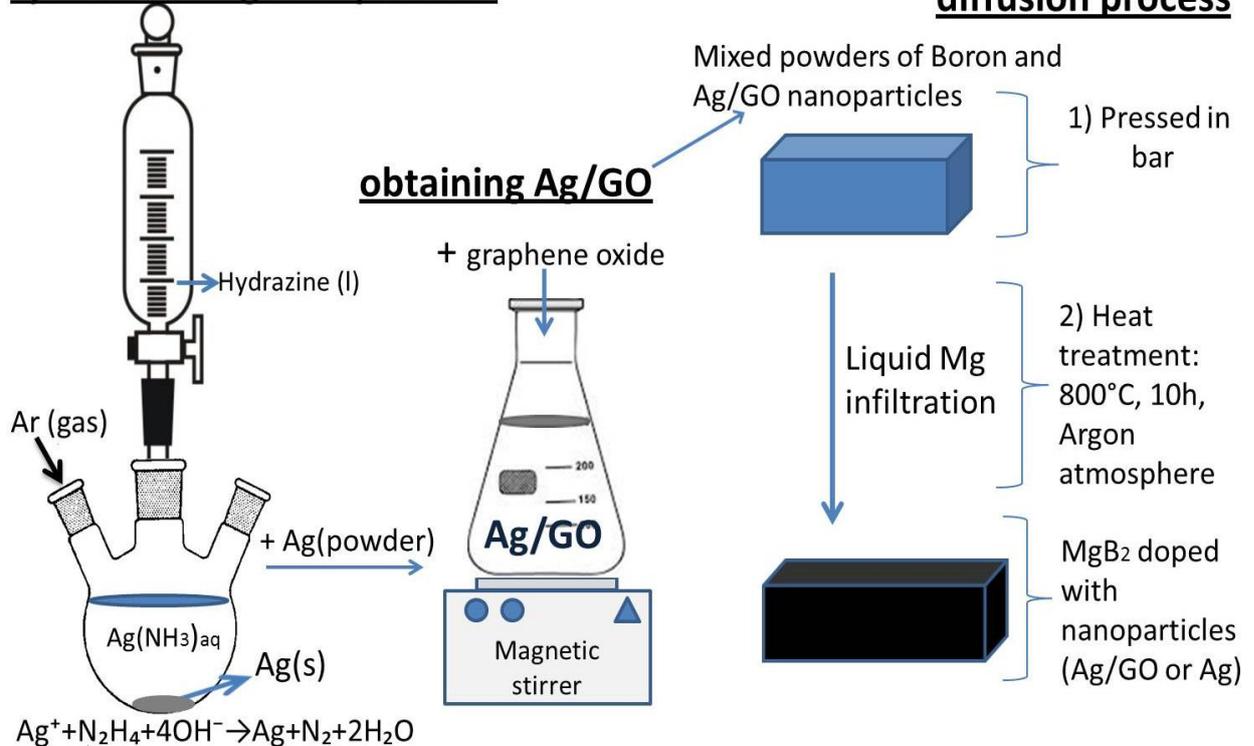
Fig. 1: Schematic illustration of sample preparation.

2.2 Nanoparticle characterization

Figure 2 shows the SEM image of as-prepared Ag nanoparticles, while the inset shows the grain size obtained from SEM images that is separated into size categories and fitted by log-normal distribution functions. The particle size is broadly distributed with the smallest particle size around 30 nm and the largest around 220 nm. Most of the particles are between 80 and 100 nm in size. Furthermore, the shapes of small particles are mostly spherical, while agglomerated particles form irregular-shaped clusters. No surfactants were used for the As–prepared Ag nanoparticles during the preparation reaction, which has a strong effect on the size distribution and shape of the particles. The lack of surfactant promotes intensified growth of nanoparticles after the nucleation process, mostly by Ostwald ripening[20].

Scanning electron microscope (SEM), atomic force microscope (AFM), and transmission electron microscope (TEM) characterizations of GO are available in our previous work[7].
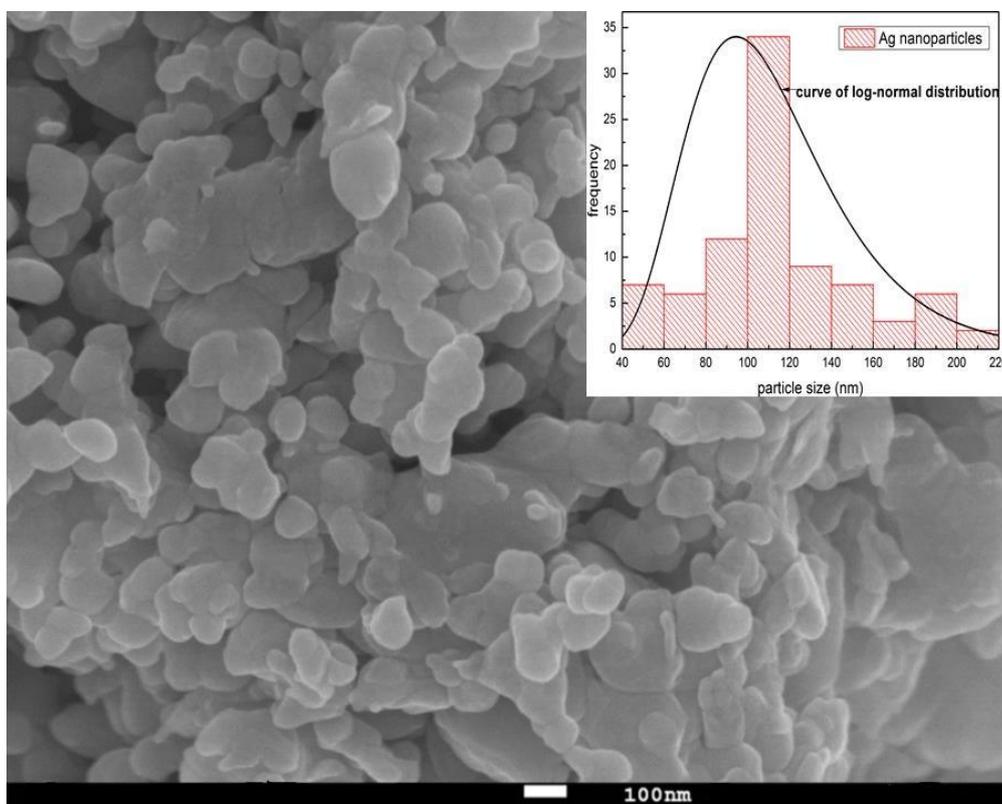
Fig. 2: The SEM image of Ag nanoparticles obtained without the use of surfactants. Inset: the log-normal size distribution obtained from the SEM image.

Figure 3 presents sheets of graphene oxide with embedded silver nanoparticles. The GO sheets contain small Ag nanoparticles with mostly spherical shape, as well as agglomerated clusters of silver particles. The smallest nanoparticles are of size below 50 nm and they are well dispersed into the GO matrix. On the other hand, larger nanoparticles have a tendency to agglomerate in clusters on GO sheets. The clusters occur most likely because of stronger Van der Walls force between the nanoparticles. The GO network partially prevents interaction between particles and thus blocks the agglomerating process upon drying into agglomerated structures (Fig. 2). Monolithic graphene is transformed by oxidation into graphene oxide with reactive functional groups such as -OH and -COOH [21]. Silver nanoparticles most likely

interact with these groups, due to electrostatic interaction, and are pinned onto the graphene oxide net.
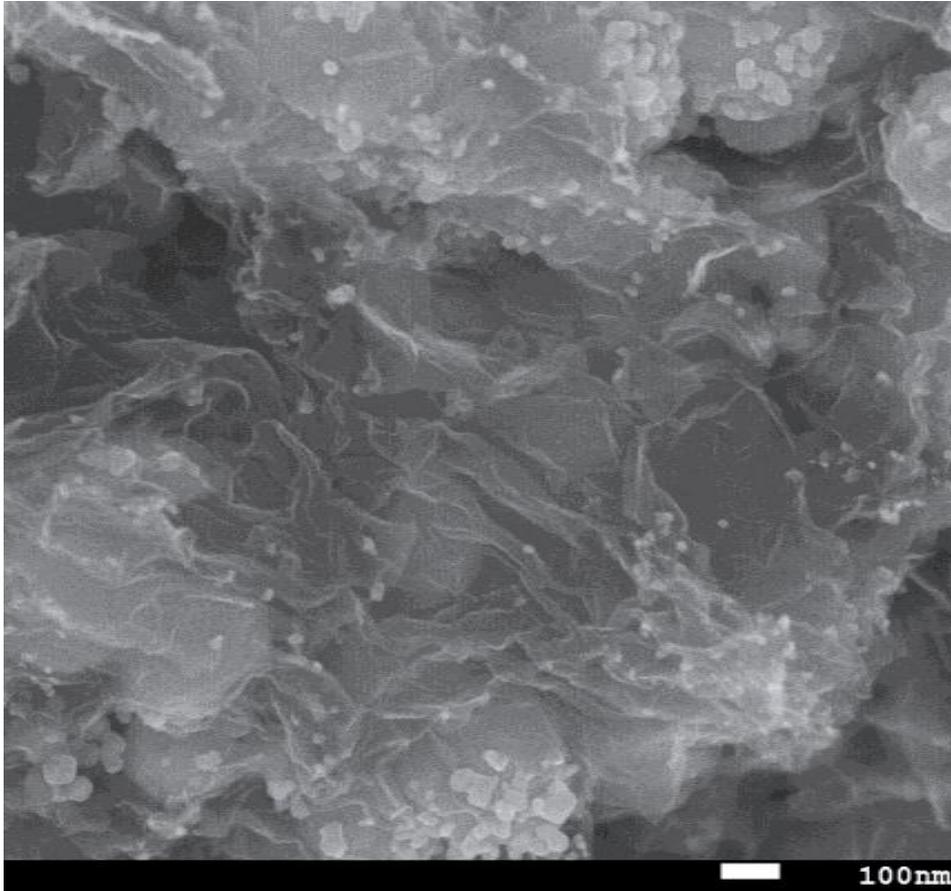
Fig. 3: SEM image of silver nanoparticles embedded on graphene oxide (GO) sheets. The image shows dispersion of Ag nanoparticles in the graphene oxide network.

The XRD pattern of the Ag nanoparticles (Fig. 4) shows that Ag nanoparticles of high purity were synthesised, with observed peaks at 38.10°, 44.09° and 64.36° (JCPDS, File No. 4-0783). On the other hand, the XRD pattern of Ag/GO shows identical peaks of Ag, with substantially more noise and two amorphous halos in region between 10 and 20°, which may indicate the presence of amorphous carbon[22]. There is no shifting of peaks observed between two patterns.
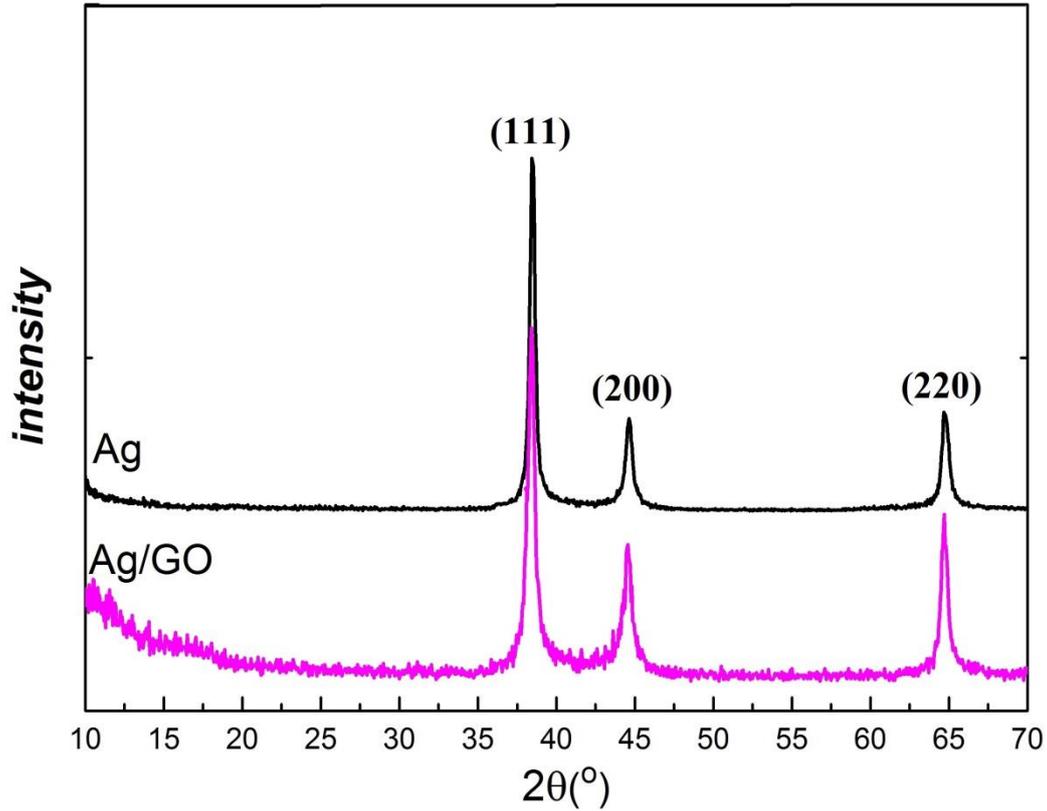
Fig. 4: XRD patterns of Ag nanoparticles and Ag/GO.

2.3. MgB$_2$ characterization

The phase identification and crystal structure investigations were carried out using an X-ray diffractometer (GBCMMA) with Cu-Kα radiation (λ = 1.54059 Å). A JEOL JSM-7500FA field emission scanning electron microscope (FESEM) was used for SEM analysis. The superconducting transition temperature, T$_C$, was determined from the magnetic ac susceptibility measurements, and the magnetic J$_C$ was derived from the width of the magnetization loop using the modified Bean model[23]. The hysteresis loops were measured by a Quantum Design Physical Properties Measurement System (PPMS). The resistivity measurements were conducted using the standard dc four-probe technique under magnetic fields up to 13 T, in the PPMS. The upper critical field (H$_{c2}$) and the irreversibility field (H$_{irr}$) were determined using the 90% and 10% criteria of R(40K) for different applied fields, where R(40 K) is the normal state resistance in the vicinity of 40 K. The active cross-section (A$_F$) was calculated from the resistivity, ρ, by Rowell's method[24].

3 Results and discussion:
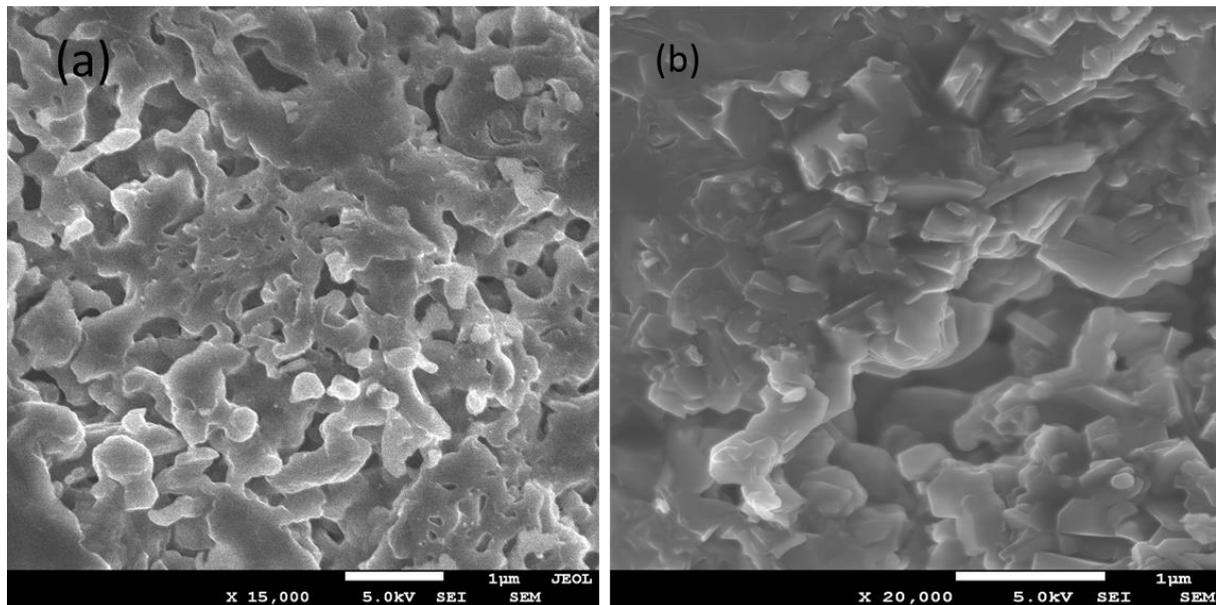
Fig. 5: SEM image of (a) non-doped MgB$_2$, and (b) MgB$_2$ doped with Ag/GO.

Figs. 5(a) and (b) show secondary electron images taken by FESEM of pure and Ag/GO doped MgB$_2$, respectively. The images indicate a rather homogeneous MgB$_2$ grain structure, with the apparent grain size around 200 nm. It gives visible evidence of the improved inter-grain connectivity in the doped sample, as the doped sample appears to be denser and to have well-connected grains compared to the non-doped sample.

The XRD measurements were performed on ground MgB$_2$ pellets. According to the Rietveld analysis of un-doped MgB$_2$ (Fig. 6 (a)), all the peaks marked with Miller indices belong to pure MgB$_2$ phase, without any other common phase as a MgO or unreacted Mg. The GO doped sample (Fig. 6 (b)) beside distinguished MgB$_2$ peaks, shows unreacted Mg peaks in relatively small amount. It is interesting that MgO phase has not been detected, indicating preservation of most GO layers between MgB$_2$ grains[6]. This is consistent with appearance of unreacted magnesium, which usually reacts with oxygen giving MgO.

Doping with nano-Ag (Fig. 7 (a)), however, has resulted in additional peaks at angles 26.88°, 38.40°, 47.51°, 55.50°, 62.6°, and 69.30° revealing the second phase as AgMg (ICDD card num. 00-029-0871) in the MgB$_2$ matrix. Similarly, Zouaoui et al.[13] have reported presence of

the same MgAg phase (ICDD card num. 00-029-0871), as well as Ag and unreacted Mg in XRD analysis of MgB_2 doped with Ag (2, 6, 16 wt.%). It is important to notice that unreacted Mg, Ag or MgO have not been detected in Ag-doped samples.

On the other hand, Ag/GO pattern (Fig. 7 (b)) presents the most complex phase composition with substantial percentage of $AgMg_3$ phase (ICDD card num. 00-001-1170) and lower percentage of AgMg phase. Beside two mentioned new phases, pure MgB_2 was mostly detected. Kumar et al.[15] also noticed $AgMg_3$ phase, and describe it as crucial pinning centres responsible for obtained high J_C. The key difference between Ag and Ag/GO doping, and consequently J_C results, were in different percentage of AgMg and $AgMg_3$ intermetallic phase. According to literature,[25] the formation mechanism of these phases is peritectic reaction during the cooling process. Formation of $AgMg_3$ is related to peritectic reaction, and occurs in very narrow part of Ag-Mg phase diagram at $X_{Mg}=0.75\sim0.80$, during the slow cooling process (liquid + MgAg $\leftrightarrow$ $AgMg_3$).

The explanation of difference in phase formation among two samples can be in GO layers. Graphene oxide sheets seem to cover silver nanoparticles, as indicated in figure 3, preventing direct reaction between Mg and Ag, due to high affinity of Ag atoms for Mg. In that case, infiltrated magnesium into boron + nanoparticles pellet need larger concentration of magnesium to penetrate in dense GO sheets and reacts with Ag. After sintering period, during the natural cooling process, higher concentration of Mg ($X_{Mg}>0.70$) promotes peristaltic reaction, and formation of $AgMg_3$ phase. Furthermore, Rietveld refinement was done using FullProf software package to determine the lattice parameters of the MgB_2 phase. The lattice parameters *a* and *c,* FWHM, micro-strain and crystallite size of all samples are given in table 1. The lattice parameters *a*, and *c* show a decreasing trend with doping for all doped samples. Rietveld refinement also provided phase distribution data, so for 2wt% GO doped sample we have 99,09 wt% of MgB_2 phase and 0.91 wt% of unreacted Mg. Ag doped sample shows

95.21wt% of pure MgB_2, 4.66wt% of AgMg, and 0.13wt% of $AgMg_3$. On the other hand, Ag/GO co-doped sample has 96.50 MgB_2 phase, 0.45wt% of AgMg, and 3.04wt% of $AgMg_3$ phase.
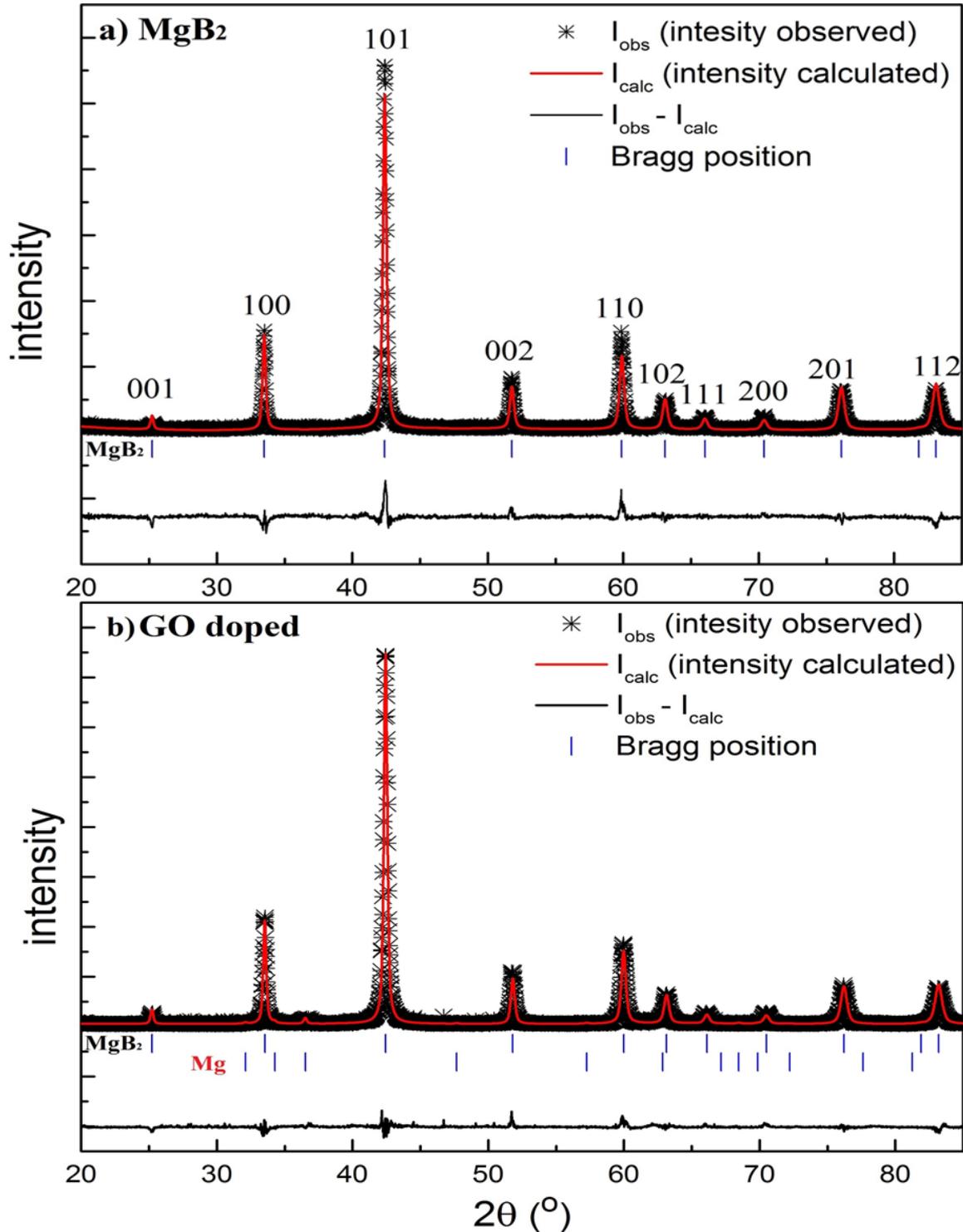
Figure 6: Fitting of XRD pattern in Rietveld refinement for pure MgB_2 (a)), GO doped MgB_2 (b)). The positions of MgB_2, Mg peaks are shown in the first, and second (b) row below the XRD patterns, respectively. Enlarged difference between the experimental XRD pattern and our fit this this pattern is shown in the bottom row.
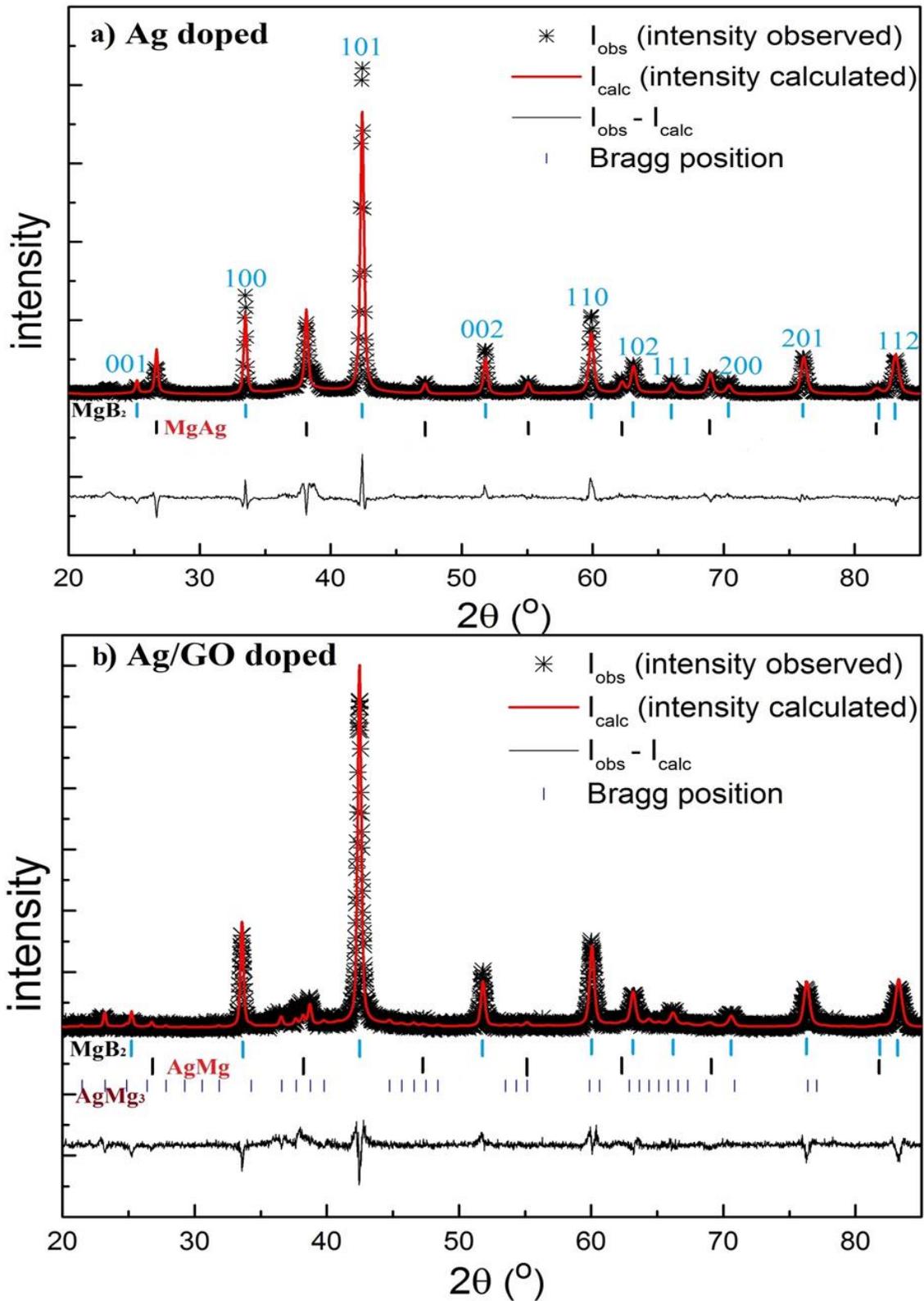
Figure 7: Fitting of XRD pattern in Rietveld refinement for Ag doped MgB_2 (a)), Ag/GO doped MgB_2 (b). The positions of MgB_2, AgMg and $AgMg_3$ peaks are shown in the first, second and third row below the XRD patterns, respectively. Enlarged difference between the experimental XRD pattern and our fit this this pattern is shown in the bottom row.

At figures 8 a), b) can be seen substantial shift of 002 and 110 diffraction peaks towards higher angels, what indicates introducing certain amount of carbon into the MgB_2 grains (intra-grain pinning) for GO and Ag/GO doped samples. These results are in good agreement with decreasing lattice parameters of all doped samples and increasing strain particularly for Ag/GO doping. Phase shifting observed at GO and Ag/GO doping is in good agreement with study of Sudesh et al.[26], where phase shifting and strain have been increased with rising GO doping from 1 to 10wt%.

On the other hand, Ag doped samples did not show any shifting in 110 and 220 reflections of MgB_2, which indicates that AgMg phase concentrates between MgB_2 grains (Fig. 8 a), b)). Yeoh et al.[6] have performed 3D atom probe tomography through the sample, and presented precise distribution of carbon and oxygen atoms, as well as location of individual GO platelets. From their study can be concluded that GO layers are uniformly dispersed in the MgB_2 matrix. Also, partially segregation of carbon and oxygen (from GO layers) has been observed, what finally enables replacing boron with carbon and cause the phase shifting.
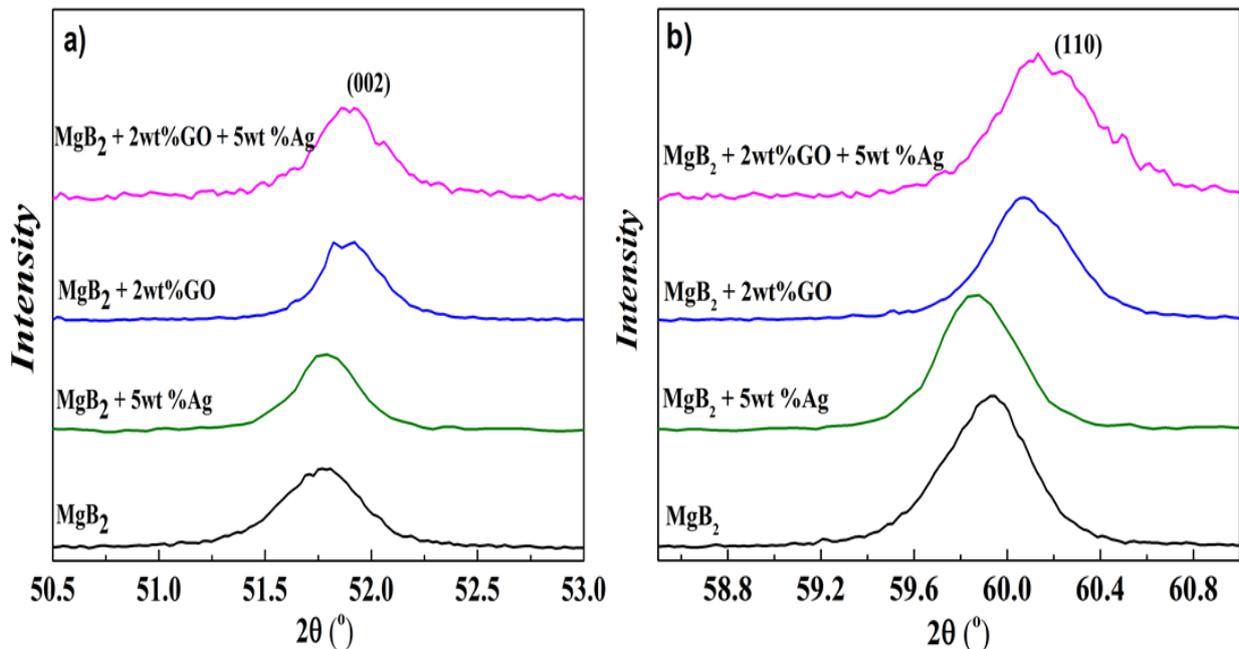
Fig. 8 a), b): Shifting of (002) and (110) peaks with GO and Ag/GO doping.

The micro-strain analysis was performed with the Williamson–Hall plot. From this plot, crystallite size and strain can be extracted from the y-intercept and gradient of the linear fit to experimental data, respectively (table 1, Fig. 9)[27]. The data was corrected for instrumental broadening using the XRD pattern of silicone standard sample.

Obtained results show increase of strain for all doped samples, with obtained strain results given in Table 1 for all samples. These results are in good agreement with strain calculation of pure MgB_2 and GO doped MgB_2 in ours previous work[7]. We could not obtain reliable values for the change of crystallite size with doping with this method, due to data scattering.
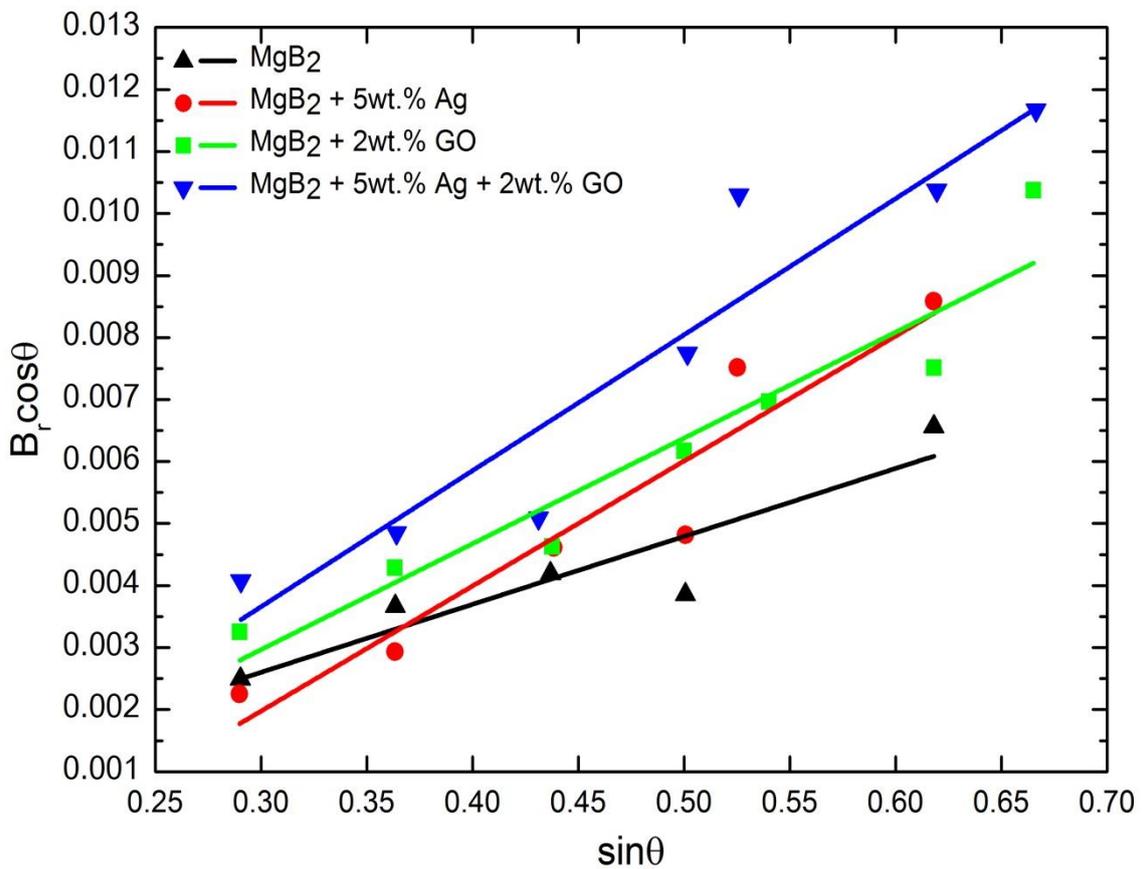
Fig. 9: Williamson-Hall plot[27] to determine lattice strain for pure MgB_2, 5wt.% Ag doped, 2wt.% GO doped, and 5wt.% Ag +2wt.% GO doped.

Sample	Lattice parameter (Å) Rietveld refainment			Strain (W-H plot) (%)
	a	*c*	*c/a*	
MgB$_2$	3.08873	3.53126	1.1433	0.1313
MgB$_2$ + 5wt% Ag	3.08859	3.52882	1.1425	0.1537
MgB$_2$ +2wt% GO	3.08473	3.52911	1.1440	0.1889
MgB$_2$ +5wt%Ag+2wt%GO	3.08087	3.52892	1.1454	0.2194

Table 1: Lattice constants *a*, and *c*, full width at half maximum (FWHM), strain, crystallite size of pure MgB$_2$, 5 wt.% Ag doped, 2 wt.% GO doped, and 5wt.% Ag + 2wt.% GO.
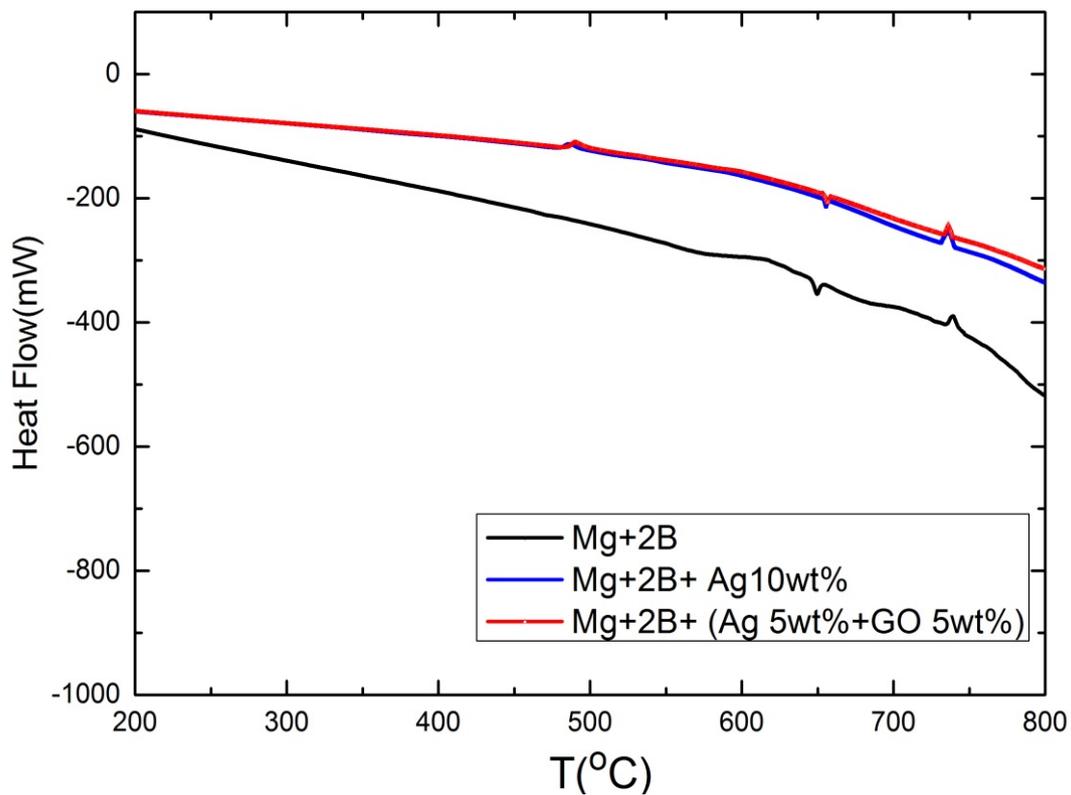
Fig. 10: DTA curve of mixed powders of Mg + 2B (bottom), Mg + 2B + Ag 10wt% (middle), and Mg + 2B + (Ag 5wt% +GO 5wt%) (top).

DTA was performed on mixed powders pressed in small bars (~200 mg) for Mg, B and Ag/GO and Ag nanoparticles, which were pressed and placed in an Al_2O_3 pan. Samples were measured as the temperature was increased up to 1000 °C at a rate of 5 K min^{-1} in an inert atmosphere of argon gas.

DTA curves (Fig. 10) show similarity with previous research on samples doped with Ni-Co-B nanoparticles[28, 29, 30]. All three observed curves have standard peaks associated with the melting of magnesium at 650ºC and the formation of MgB_2 at 750ºC. Doped samples have additional peak at 480ºC that is related to formation of a eutectic system between Ag nanoparticles and magnesium. According to Ag-Mg phase diagram, AgMg phase is dominant in the range 30-80 at.% of magnesium and up to temperature of 820 ºC, while in a narrow phase range (X_{Mg}>75-80%) formation of $AgMg_3$ has occurred up to temperature of 469ºC [25, 31].

Creation of this type of Mg-Ag compounds strongly depends on the particular composition and percentages of elements especially for nano-sized materials. Formation of the eutectic system has been reported for many other types of nanoparticle doping [28, 32, 33]. It is important to note that in preparation of samples for DTA analysis, all starting materials are pre-mixed together and measured. This is quite different than the diffusion method where just boron and nanoparticles are mixed together and pressed into a bar, while liquid magnesium starts to infiltrate into the pre-mixed bar at $\leq$ 650 °C. Finally, in the diffusion technique of MgB_2 growth, creation of $MgAg_3$ phase can occur only by cooling process in peritectic reaction.

sample	T_C (K)	$\rho(300K)$ ($\mu\Omega cm$)	$\rho(40K)$ ($\mu\Omega cm$)	RRR ($\mu\Omega cm$)	A_F %	H_{c2} at25K (T)	H_{irr} at25K (T)
Non-doped MgB$_2$	38.9	47.02	12.74	3.69	21.4	9.4	7.6
MgB$_2$ + 5wt% Ag	38.15	35.87	10.26	3.5	28.0	9.4	7.6
MgB$_2$ +2wt% GO	37.7	21.4	9.08	2.36	59.0	11.1	8.5
MgB$_2$ +5wt%Ag+2wt%GO	36.3	61.57	32.71	1.88	25.0	12.4	9.1

Table 2: Critical temperature (Tc), resistivity at 300K and 40K, residual resistivity ratio (RRR), active cross-section (A_F), upper critical field (H_{c2}), and irreversibility field (H_{irr}) of non-doped, Ag doped, GO doped, and Ag + GO co-doped bulk samples.

Table 2 presents the critical temperature, resistivity at 300 K and 40 K, the residual resistivity ratio (RRR) and the active cross-sectional area (A_F) of the non-doped, nano-Ag doped, GO-doped and co-doped MgB$_2$ bulk samples. Considerable T_C degradation[34] and the presence of impurity phases[35] can be observed. It is worth noting, however, that the reduction of T_c due to nano-Ag addition is low compared to carbon dopants at the same level of doping[2, 3, 4]. The samples doped with 5wt.% nano-Ag and 2wt.% GO showed low resistivity values, however, the co-doped samples showed a much higher resistivity value. The presence of impurity phases and the substitution of carbon onto boron sites are believed to be responsible for the increase in the resistivity in the co-doped sample. Because Ag nanoparticles got dispersed evenly through the sample due to the presence of GO (Fig. 1), these nanoparticles may have introduced strain field into MgB$_2$ grains throughout the sample. This would then result in the observed increased resistivity of Ag/GO co-doped MgB$_2$. The smaller observed A_F than for GO-doped MgB$_2$ is consistent with this picture (Table 2), as Ag nanoparticles also cause local grain misalignment. Based on our previous work, GO seems to provide a platform for uniform nucleation of MgB$_2$ grains, which has resulted in a remarkable improvement in the inter-grain connectivity with higher active cross section area (A_F)[6]. GO doping does not result

in increased resistivity due to inter-and intra-band scattering, which would be expected for carbon-doping[8]. The lower than expected resistivity of the GO-doped sample occurs because of the prevailing effect of improved grain connectivity. GO was dispersed evenly through the MgB_2 sample, producing no agglomerates that would disturb the MgB_2 grain connectivity.

The residual resistivity ratio (RRR) gives an indication on the disorder in the sample, so the decreased RRR values compared with the non-doped sample reflect the influence of doping on increasing the defects in MgB_2 crystals[36]. Addition of Ag nanoparticles decreased RRR value very little indicating that the Ag nanoparticles didn't disperse enough to produce substantial defects in the MgB_2 crystals. This was expected, as no surfactants were used for the nanoparticles and they lumped together. GO doping decreased RRR by about 35%, introducing the defects through carbon substitution.[2-7,26] GO + Ag co-doping decreases the value of RRR by about 50%. Ag nanoparticles were dispersed on GO sheets, making them much more effective in creation of defects, in addition to the defects introduced by the C released from surface of GO sheets. Strongly increased value of resistivity with the co-doping is consistent with the strongly decreased value of RRR. This also correlates well with the observed higher H_{c2} and H_{irr} values of the co-doped samples compared to the non-doped and other doped samples, owing to higher intra-band impurity scattering due to defects introduced by co-doping.

Figure 11 shows the field dependence of J_C of the pure MgB_2 and Ag doped samples at 5 and 20K. In this particular research, optimization of doping with Ag nanoparticles was conducted, with doping at 2.5, 5, and 7.5 wt%. All three doped samples showed improvement of critical current density in comparison with the pure sample, but with small differences among themselves. Among the doped samples, 5 wt% Ag doping gives the largest value of J_C, measured at both 5 and 20 K. The present values of J_C are in the range of common results for samples doped with silver.
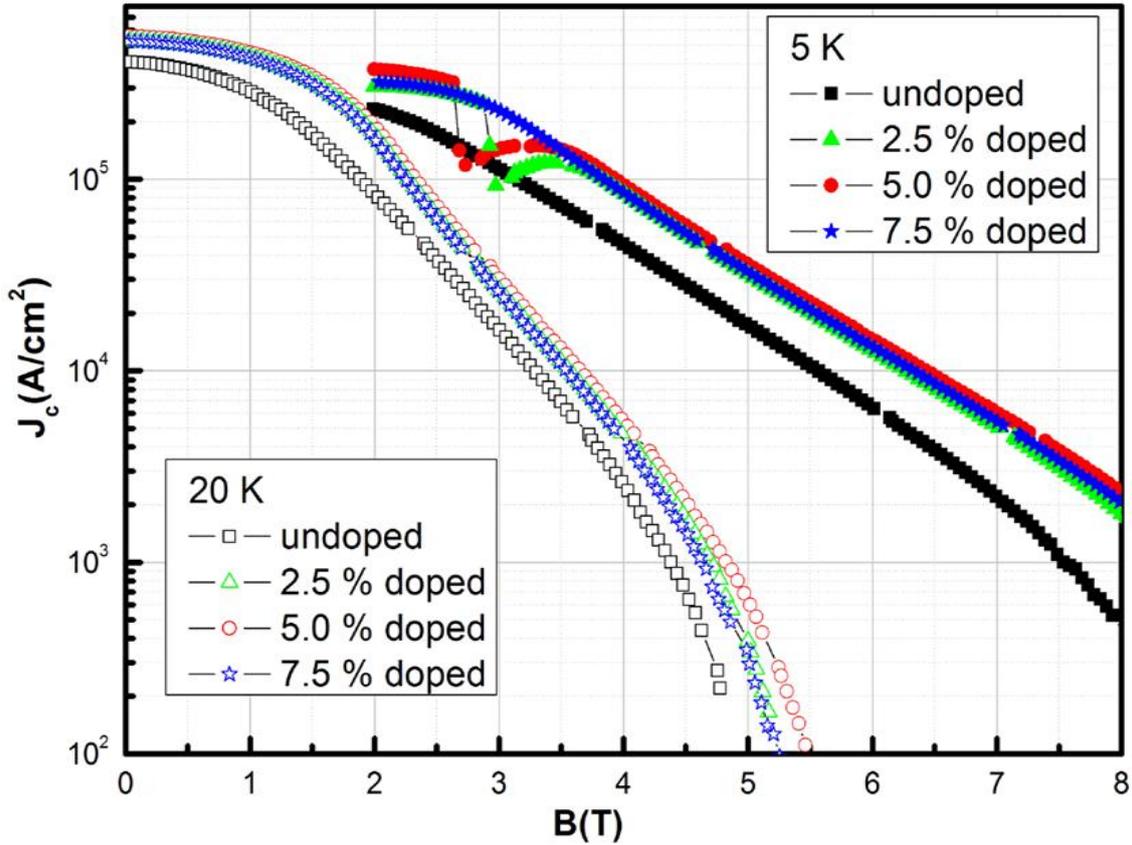
Fig 11: Field dependence of critical current density of pure and Ag doped samples.

Figure 12 shows the in-field J_C performance at 5 and 20 K for non-doped, nano-Ag doped, GO doped, and nano-Ag/GO co-doped bulk samples of MgB_2. The J_C curves for the doped and co-doped samples show a significant improvement over the non-doped sample at both 5 and 20 K. The sample with 1 wt.% GO showed a J_C of 6.35×10^5 Acm^{-2} at 20 K under zero field. As reported by Li et al.[37] a strong correlation exists between the connectivity and the self-field J_C, so better grain connectivity and higher A_F values gives higher self-field J_C values. On the other hand, high field J_C performance is manly governed by H_{c2} and the flux pinning. The sample co-doped with nano-Ag and GO shows a remarkable value of J_C, 6.08 $\times 10^4$ A/cm^2 at 5 K, 8 T, which is comparable to the highest J_C ever reported for bulk MgB_2 samples. Some level of carbon substitution on boron sites and the presence of nano size $AgMg_3$ impurity phase have significantly improved J_C at high fields, through enhanced H_{c2} and flux pinning. As can be seen the Ag/GO doped sample has a lower value of J_C at low

magnetic field than the GO doped sample due to its having considerably more impurities (Ag + GO).
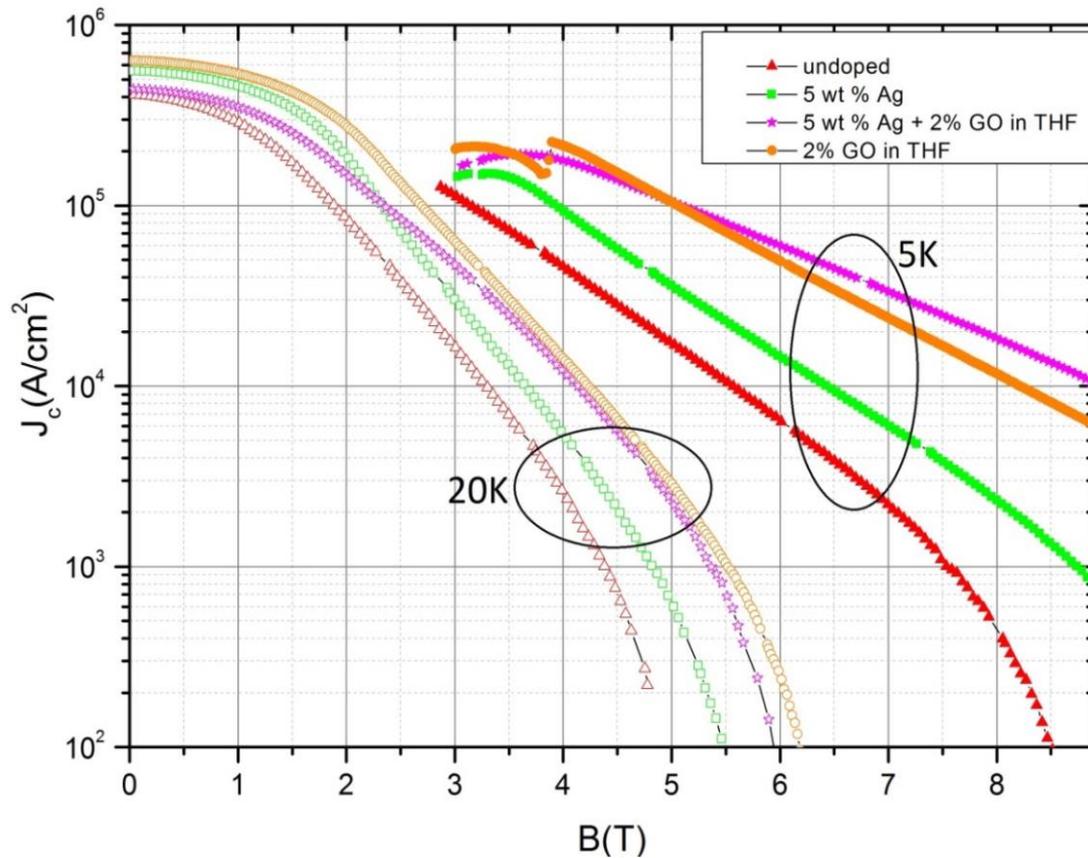
Fig 12: Field dependence of critical current density obtained for pure MgB_2, and the Ag doped, GO doped, and Ag/GO co-doped MgB_2 samples.

4. Conclusion

In this work we present a systematic study of the effects of Ag and GO co-doping on the critical current density, crystallinity, and resistivity of MgB_2 bulk samples. The GO/Ag co-doping remarkably improved J_C properties under high fields and enhanced the critical fields. The obtained results are among the best achieved for any doped MgB_2 samples. Ag/GO co-doping has several advantages. GO helps disperse as-prepared Ag nanoparticles in MgB_2, so that Ag nanoparticles homogenously react with Mg and create affective pinning centres $AgMg_3$ and AgMg in MgB_2 creating efficient intra- and inter-grain pinning, while in the

same time not having significant deleterious effect on grain connectivity. The formation of $AgMg_3$ phase (for Ag/GO co-doped MgB_2) is crucial factor of improvement of vortex pinning in MgB_2, especially enhancing superconducting performance at high magnetic fields.

On the other hand, GO promotes alignment of MgB_2, improving the grain connectivity. Carbon from GO seems to be incorporate into MgB_2 (replacing boron), and additionally improving the flux pinning. Furthermore, AgMg phase was significantly present in Ag doping, but with considerably less effect on the flux pinning in comparison to Ag/GO co-doping.

Diffusion method provides maximal efficient reactivity of magnesium trough sample with less vacancies caused by melting magnesium then in-situ prepared samples providing denser sample with better connectivity among grains, while GO net provides uniform dispersion of doped materials. In comparison with previous research by other groups, Ag/GO co-doping significantly improves the critical current results, especially at high magnetic field, shifting the limits of MgB_2 applications.

Acknowledgements:

REFERENCES:

[1] Nagamatsu J.; Nakagawa N.; Muranaka T.; Zenitani Y.; Akimitsu J.; Superconductivity at 39 K in Magnesium Diboride. *Nature*, **2001**, *410*, 63–64.

[2] Yeoh W.K., Kim J.H., Horvat J., Dou S. X., Munroe P.; Improving Flux Pinning of MgB$_2$ by Carbon Nanotube Doping and Ultrasonication. *Supercond. Sci. Technol.*, **2006**. *20(2)*, 5.

[3] Dou S.X.; Shcherbakova O.; Yeoh W.K.; Kim J.H.; Soltanian S.; Wang X.L.; Senatore C.; Flukiger R.; Dhalle M.; Husnjak O.; Babic E.; Mechanism of Enhancement in Elektromagnetic Properties of MgB$_2$ by Nano SiC Doping. *Phys. Rev. Lett.* **2007**, *98(9)*, 097002.

[4] J.H. Kim, S. Zhou, M.S.A. Hossain, A.V. Pan, S.X. Dou, Carbohydrate Doping to Enhance Electromagnetic Properties of MgB$_2$ Superconductors. *Appl. Phys. Lett.* **2006**, *89(14)*, 142505-3.

[5] Xu X.; Dou S.X.; Wang X. L.; Kim J. H.; Choucair M.; Yeoh W. K.; Zheng R.K.; Ringer S.P.; Graphene Doping to Enhance the Flux Pinning and Supercurrent Carrying Ability of a Magnesium Diboride Superconductor. *Supercond. Sci. Technol..* **2010**, *23(8)*, 085003.

[6] Yeoh W.K.; Cui X.Y.; Gault B.; De Silva K.S.B.; Xu X.; Liu H.W.; Yen H.W.; Wong D.; Bao P.; Larson D.J.; et al. On the Roles of Graphene Oxide Doping for Enhanced Supercurrent in MgB$_2$ Based Superconductors. *Nanoscale*, **2014**, *6(11)*, 6166-6172.

[7] De Silva K.S.B.; Aboutalebi S.H.; Xu X.; Wang X.L.; Li W.X.; Konstantinov K.; Dou S.X.; A Significant Improvement in Both Low- and High-Field Performance of MgB$_2$ Superconductors Through Graphene Oxide Doping. *Scr. Mater.* **2013.** 69(6); 437-440.

[8] Zhang Y.; Dou S.X.; Lu C.; Zhou S.H.; Li W.X.; Effect of Mg/B Ratio on the Superconductivity of MgB$_2$ Bulk with SiC Addition. *Phys. Rev. B*, **2010**, *81(9)*, 094501.

[9] Shekhar C.; Giri R.; Tiwari R.S.; Srivastava O.N.; Malik S.K.; High Critical Current Density and Improved Flux pinning in Bulk MgB$_2$ Synthesized by Ag Addition. *J. Appl. Phys*, **2007**, *101(4)*: 043906-043906-6.

[10] Grivel J.C.; Abrahamsen A.; Bednarčík J.; Effects of Cu or Ag Additions on the Kinetics of MgB$_2$ Phase Formation in Fe-Sheathed Wires. *Supercond. Sci. Technol.* **2008**, *21(3)*, 035006.

[11] Xu X.; Dou S.X.; Wang X.L.; Kim J. H.; Stride J. A.; Choucair M.; Yeoh W.K.; Zheng R.K.; Ringer S.P.; Graphene Doping to Enhance the Flux Pinning and Supercurrent Carrying Ability of a Magnesium Diboride Superconductor. *Supercond. Sci. Technol.* **2010**. *23(8)*, 085003.

[12] Sun T.; Zhang X. P.; Zhao Y. G.; Shen R.; Wang K.; Zhang L. W.; Cao B. S.; Xiong Y. H.; Li P. J.; Wen H. H.; Study of the Reactions Between MgB$_2$ and Ag at High Temperature, *Physica C.* **2002**, *382*, 367.

[13] Zouaoui M.; M'chirgui A.; Ben Azzouz F.; Yangui B.; Ben Salem M.; Electron Transport Properties of Silver Added Polycrystalline MgB$_2$. *Physica C.* **2002**, *382*, 217–223.

[14] Toulemonde P.; Musolino N.; Flukiger R.; High-Pressure Synthesis of Pure and Doped Superconducting MgB$_2$ Compounds. *Supercond. Sci. Technol.* **2003**, *16*, 231.

[15] Kumar D; Pennycook S. J.; Narayan J.; Wang H.; Tiwari A.;, Role of Silver Addition in the Synthesis of High Critical Current Density MgB$_2$ Bulk Superconductors. *Supercond. Sci. Technol.* **2003**, *16*, 455–458.

[16] Song K. J.; Kim S. W.; Park C.; Chung J. K.; Yang J. S.; Joo J. H.; Ko R. K.; Ha H. S.; Kim H. S.; Ha D. W.; et al. The Effect of Nano-Powder Additions on the Superconducting Properties of MgB$_2$. *IEEE Trans. Appl. Supercond.* **2005**, *15*, 3288.

[17] Shimoyama J.; Hanafusa K.; Yamamoto A.; Katsura Y.; Horii S.; Kishio K.; Kumakura H.; Catalytic Effect of Silver Addition on the Low Temperature Phase Formation of MgB$_2$. *Supercond. Sci. Technol.* **2007**, *20*, 307–311.

[18] Kimishima Y.; Takami S.; Uehara M.; Numa S.; Sugiyama Y.; Kuramoto T.; Pinning Properties of Ag/MgB$_2$ Bulk System. *Physica C*. **2008**, *468*, 1181–1184.

[19] Ranot M.; Seong W.K.; Jung S.-G.; Lee N.H.; Kang W.N.; Joo J.H.; Zhao Y.; Dou S.X.; Enhancement of the Critical Current Density of MgB$_2$ Thick Films by Ag-and Cu-Impurity Layers. *Physica C*. **2009**, *469*, 1563–1566.

[20] Ostwald W.; *Lehrbruck der Allgemeinen Chemie*. **1896**, *2*, 1.

[21] Sun L.; Fugetsu B.; Mass Production of Graphene Oxide from Expanded Graphite. *Maters. Lett*. **2013**, *109*, 207–210.

[22] Cui, P.; Lee, J.; Hwang, E.; Lee, H. One-Pot Reduction of Graphene Oxide at Subzero Temperatures, *Chem. Commun.*, **2011**, *47*, 12370–12372.

[23] Bean C.P.; Magnetization of High-Field Superconductors. *Rev. Mod. Phys*. **1964**, *36*, 31-39.

[24] Rowell J.M.; The Widely Variable Resistivity of MgB$_2$ Samples; *Supercond. Sci. Technol*. **2003**, *16(6)*, R17.

[25] Cahn R.W.; Haasen P; Physical Metallurgy, *Elsevier science*, **1996**, *1*, 492.

[26] Sudesh, Kumar N.; Das S.; Bernhard C.; Varma G. D.; Effect of Graphene Oxide Doping on Superconducting Properties of Bulk MgB$_2$. *Supercond. Sci. Technol*. **2013,** *26*, 095008.

[27] Williamson G K and Hall W H, X-ray Line Broadening from Filed Aluminium and Wolfram; *Acta Metall*. **1953**, *1*, 22-31.

[28] Mustapić M.; Horvat J.; Hossain M. S.; Skoko Ž.; Sun Z.; Mitchell D.R.G.; Dou S. X.; Novel Synthesis of Superparamagnetic Ni–Co–B Nanoparticles and Their Effect on Superconductor Properties of MgB$_2$. *Acta Mater*. **2014**, *70*, 298–306.

[29] Mustapić M.; Horvat J.; Hossain M. S.; Skoko Ž.; Dou S. X.; Interplay Between Boron Precursors and Ni-Co-B Nanoparticles Doping in the Fabrication of MgB$_2$ Superconductor with Improved Electromagnetic Properties. *Acta Mater*. **2014**, *80,* 457–467.

[30] Mustapić M.; Horvat J.; Hossain M. S.; Skoko Ž.; Dou S. X.; Enhancing Superconducting Properties of MgB$_2$ Pellets by Addition of Amorphous Magnetic Ni–Co–B nanoparticles. *Supercond. Sci. Technol*. **2013**, *26*, 075013.

[31] Zemczuznyj S.F.; On the Alloys of Magnesium with Silver. *Z. Anorg. Chem*. **1906**, *49*, 400-414.

[32] Chen S.K.; Lockman Z.; Wei M.; Glowacki B.A.; MacManus-Driscoll J.L.; Improved Current Densities in MgB$_2$ by Liquid-Assisted Sintering;; *Appl. Phys. Lett*. **2005,** *86*, 242501.

[33] Grivel J-C.; Andersen N.H.; Pallewatta P.G.A.P.; Zhao Y.; Zimmermann M.; Influence of Bi, Se and Te Additions on the Formation Temperature of MgB$_2$, *Supercond. Sci. Technol*. **2012,** *25,* 015010.

[34] Teruo M.; Kiuchi M.; Yamamoto A.; Shimoyama J.; Kohji K.; Essential Factors for the Critical Current Density in Superconducting MgB$_2$: Connectivity and Flux Pinning by Grain Boundaries. *Supercond. Sci. Technol*. **2008**, *21(1)*, 015008.

[35] Wilke R. H. T.; Budko S. L.; Canfield P. C.; Finnemore D. K.; Suplinskas R. J.; Hannahs S. T.; Systematic Effects of Carbon Doping on the Superconducting Properties of Mg(B$_{1x}$C$_x$)$_2$. *Phys. Rev. Lett*. **2004**, *92(21)*, 217003.

[36] Wang X.-L.; Dou S.X.; Hossain M.S.A.; Cheng Z.X.; Liao X.Z.; Ghorbani S.R.; Yao Q.W.; Kim J.H.; Silver T.; Enhancement of the In-Field J$_C$ of MgB$_2$ via SiCl$_4$ Doping. *Phys. Rev. B*. **2010**. *81(22)*, 224514.

[37] W. X. Li, Y. Li, R. H. Chen, R. Zeng, S. X. Dou, M. Y. Zhu, and H. M. Jin, "Raman Study of Element Doping Effects on the Superconductivity of MgB$_2$," *Phys. Rev. B* 77, 094517, 2008.

Table of Contents